Accuracy evaluation of on-wafer load-pull measurements

AIMETA 2017
XXIII Conference
The Italian Association of Theoretical and Applied Mechanics
Luigi Ascione, Valentino Berardi, Luciano Feo, Fernando Fraternali and Antonio Michele Tralli (eds.)
Salerno, Italy, 4–7 September 2017

THERMAL DISTRIBUTION IN CANCEROUS BREAST WITH ANISOTROPIC PROPERTIES VIA A SEMI-ANALYTICAL HOMOGENIZATION APPROACH

Ariel Ramírez-Torres[1], Alfio Grillo[1], Luigi Preziosi[1], Reinaldo Rodríguez-Ramos[2], Julián Bravo-Castillero[2], Raúl Guinovart-Díaz[2], and Federico J. Sabina[3]

[1]Dipartimento di Scienze Matematiche "G. L. Lagrange"
Politecnico di Torino, 10129. Torino, Italia
e-mail: torres@calvino.polito.it, alfio.grillo@polito.it, luigi.preziosi@polito.it

[2] Departamento de Matemáticas, Facultad de Matemática y Computación
Universidad de La Habana, CP 10400, La Habana, Cuba
e-mail: reinaldo@matcom.uh.cu, jbravo@matcom.uh.cu, guino@matcom.uh.cu

[3] Instituto de Investigaciones en Matemáticas Aplicadas y en Sistemas (IIMAS)
Universidad Nacional Autónoma de México, 01000 CDMX, Apartado Postal 20-126, México
e-mail: fjs@mym.iimas.unam.mx

Keywords: heterogeneous breast cancer, thermography, asymptotic homogenization, anisotropic thermal conductivity

Abstract. *Cancer is the second leading cause of death worldwide and breast cancer is one of the most frequently diagnosed cancers. Nowadays, thermography technique has emerged as a noninvasive and prospective method to complement mammography and to improve the efficiency of early and overall detection of breast cancer. In this work, analytical and numerical strategies are employed to solve a bioheat transfer equation with rapidly oscillating coefficients. The macroscale thermal conductivity is computed by applying the asymptotic homogenization technique, the local cell problem is solved analytically and the macro-scale problem is solved via finite element method. We considered thermal anisotropy and found that it provides extra information regarding the thermal profile on the breast surface near the cancerous area.*

1 INTRODUCTION

Cancer is the second leading cause of death worldwide and breast cancer is one of the most frequently diagnosed. Particularly, fibroadenoma is the most common surgically treated breast mass in adolescents, accounting for 44-94% of biopsied breast lesions [1] and it has been found out that fibroadenomas raise the breast surface temperature so that it can be detected using thermal imaging [2]. Breast infrared thermography is a noninvasive procedure that does not involve compression of the breast tissue or exposure to radiation, and works through an assessment of physiological functions, via high resolution surface temperature measurements [3, 4]. Mammography and ultrasound are ones of the most used clinical protocols employed to detect and provide a diagnosis of breast cancer. However, they present a range of known limitations (see e.g. [5]). Then, a combination of therapies that incorporates thermography may boost both sensitivity and specificity. In several works the temperature distribution over breasts with and without tumors have been studied, wherein heat transfer in the biological tissue is modeled using Pennes bioheat equation [6]. For instance, we can cite the works [7, 8, 9], among others. In a recent work [9], we took into account the heterogeneity of the tumor and studied its influence on the breast surface temperature. Particularly, we observed that the increase of the cancerous tissue volume fraction induces an augment in the breast surface temperature.

In the present work we aim to extend the model in [9] by considering an anisotropic conductivity tensor. Likewise, the breast is supposed to be a multilayered structure consisting of muscle, fat and gland, where the cancerous region is considered embedded in the glandular tissue. Analytical and finite element computations are integrated to solve the bioheat transfer equation with rapidly oscillating coefficients. In this sense, the macroscale thermal conductivity is computed by applying the asymptotic homogenization technique [10, 11] exploiting the sharp length scale separation between the local malignant hetereogeneities and the characteristic size of the whole tissue. Specifically, the local cell problem is solved analytically by using a procedure analogous to that in [12], but formulating conveniently the cell problems. Finally, the macro-scale problem is solved via finite element method. Numerical results show that the consideration of anisotropy induces temperature profile alterations in the region near the tumor and on the breast surface. Actually, the fundamental importance of including anisotropic properties on tumor progression have been demonstrated [13, 14]. For example, in [13] the authors propose a continuous mechanical model for simulating the invasion of the glioblastoma multiforme and use medical images to introduce the diffusion tensor presenting an anisotropic form.

2 PHYSICAL MODEL

Woman's breasts are considered to present different density compositions and can be divided into four categories, namely, extremely dense (ED), heterogeneously dense (HD), scattered fatty (SF) and predominantly fatty (PF) [15]. Here, we focus on the ED case, that is when the breast is considered to have a higher composition of fibrous and connective tissues with low fatty tissue content. Moreover, we modeled the cancerous breast cross-section composed by muscle, glandular and fat tissues (denoted by Ω_m, Ω_g and Ω_f, respectively) and the tumorous region is assumed to be encapsulated, round, and composed by glandular and fibrous tissue (in fact, fibroadenomas present this structure [16]). The heterogeneous tissue is characterized by two regions of different thermophysical properties: the glandular tissue (Ω_g^ε) and a periodically square lattice of arranged circular cancerous inclusions (Ω_c^ε) (see Fig. 1). We emphasize that our model is two-dimensional.

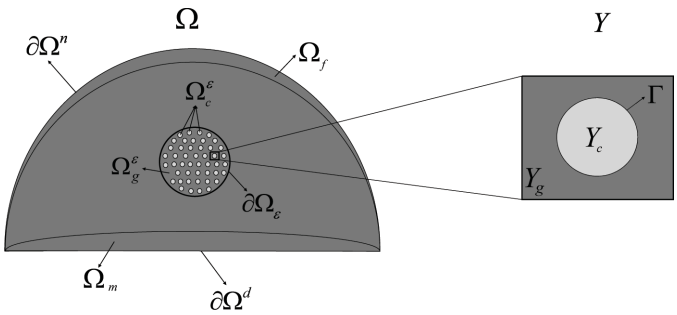

Figure 1: Decomposition of the macroscopic two-dimensional domain (left) and the corresponding unit periodic cell (right). The breast cross-section is assumed to be hemispherically shaped with a diameter $L = 0.14\ m$. The cancerous region will consist of a periodic microstructure associated with the open, bounded and connected domain $\Omega_\varepsilon = \Omega_g^\varepsilon \cup \Omega_c^\varepsilon \cup \partial\Omega_\varepsilon$. The reference periodic cell will be denoted by Y, which contains a cancerous inclusion occupying the domain Y_c such that $Y = Y_g \cup Y_c \cup \Gamma$, with $\overline{Y}_c \subset Y$ and $Y_g \cap Y_c = \emptyset$. Then, the cancerous breast is represented by $\Omega = \Omega_m \cup \Omega_g \cup \Omega_\varepsilon \cup \Omega_f$.

3 MATHEMATICAL STATEMENT OF THE PROBLEM

The aim is to find the temperature fields described by Pennes bioheat transfer equation [6],

$$(\mathcal{P}^i) \quad \rho^i c^i \frac{\partial u^i}{\partial t} = \nabla \cdot \left(\boldsymbol{k}^i \nabla u^i\right) - \rho_b c_b \omega_b^i (u^i - u_a) + q_m^i \quad \text{in } \Omega_i \times (0,T), \tag{1}$$

where the index $i = m, g, f, \varepsilon$ indicates that the specified variable belongs to the corresponding Ω_i domain, u_a is the arterial blood temperature and ρ_b and c_b are the density and the specific heat capacity of blood, respectively. In addition, tissue density, specific heat, thermal conductivity, blood perfusion and metabolic heat generation are given by ρ^i, c^i, $\boldsymbol{k}^i$, ω_b^i and q_m^i, respectively for each domain Ω_i. Particularly, the rapidly oscillating material coefficients $\boldsymbol{k}^\varepsilon$, ω_b^ε and q_m^ε, are supposed to be piecewise constant and defined by,

$$\boldsymbol{k}^\varepsilon = \begin{cases} \operatorname{diag}[k_1^g, k_2^g], & \mathbf{x} \in \Omega_g^\varepsilon \\ \operatorname{diag}[k_1^c, k_2^c], & \mathbf{x} \in \Omega_c^\varepsilon \end{cases}, \quad \omega_b^\varepsilon = \begin{cases} \omega_b^g & \mathbf{x} \in \Omega_g^\varepsilon \\ \omega_b^c & \mathbf{x} \in \Omega_c^\varepsilon \end{cases} \quad \text{and} \quad q_m^\varepsilon = \begin{cases} q_m^g & \mathbf{x} \in \Omega_g^\varepsilon, \\ q_m^c & \mathbf{x} \in \Omega_c^\varepsilon, \end{cases}$$

where k_1^j, k_2^j, ω_b^j and q_m^j $(j = g, c)$ are constants.

Boundary conditions for equation (1) are heat transfer by convection between the surface of the tissue and the external environment on $\partial\Omega^n$ and a prescribed temperature value on $\partial\Omega^d$,

$$\begin{aligned} -\boldsymbol{k}^f \nabla u^f \cdot \mathbf{n} &= h\left(u^f - u_e\right) && \text{on } \partial\Omega^n \times (0,T), \\ u^m &= u_p && \text{on } \partial\Omega^d \times (0,T), \end{aligned}$$

where h denotes the combined effective heat transfer coefficient due to convection, radiation and evaporation, u_e is the surrounding temperature and u_p is a prescribed temperature between the breast and the chest. The initial condition is

$$u^i = \tilde{u} \quad \text{in } \Omega \text{ for } T = 0.$$

Moreover, heat flux and temperature continuity at the interface of the tissue layers is imposed and described by the following equations

$$\boldsymbol{k}^i \nabla u^i \cdot \mathbf{n} = \boldsymbol{k}^{i+1} \nabla u^{i+1} \cdot \mathbf{n}, \tag{2}$$

$$u^i = u^{i+1}, \tag{3}$$

as well as in the circular interface Γ in the periodic cell, i.e.,

$$[\![u^\varepsilon]\!] = 0 \quad \text{and} \quad [\![\boldsymbol{k}^\varepsilon \nabla u^\varepsilon \cdot \mathbf{n}]\!] = 0 \quad \text{on } \Gamma,$$

where $[\![\bullet]\!]$ denotes the contrast across the interface taken from the matrix to the inclusions. In (2) and (3) the following order must be understood $\{i,j\} = \{\{m,g\},\{g,\varepsilon\},\{g,f\}\}$.

4 SOLUTION PROCEDURE

It can be noted from Fig. 1 that problems $(\mathcal{P}^i)$ $(i \neq \varepsilon)$ are already set in a macro-scaled framework. On the other hand, in the heterogeneous tissue (the cancerous area), we must first deal with problem $(\mathcal{P}^\varepsilon)$ via asymptotic homogenization technique in order to obtain a homogenized representation of it (denoted by $(\mathcal{P}^h)$). Macroscale boundary conditions are then found for the homogenized problem allowing us to coupled it with $(\mathcal{P}^i)$. Finally, we can merged the coupled macro problems (that is $(\mathcal{P}^i)$ and $(\mathcal{P}^h)$) into a single one and solve it numerically.

4.1 Homogenization technique

The homogenized formulation of $(\mathcal{P}^\varepsilon)$ in the heterogeneous tissue Ω_ε can be obtained by applying the two-scale homogenization technique ([10, 11]). With this aim, let $\varepsilon > 0$ be the size of the microstructure and introduce the fast scale coordinate $\mathbf{y} = \mathbf{x}/\varepsilon$. An asymptotic expansion of u^ε is sought as a function of ε for $\varepsilon \to 0$ in the form

$$u^\varepsilon(\mathbf{x}) = u_0(\mathbf{x},\mathbf{y}) + \varepsilon u_1(\mathbf{x},\mathbf{y}) + \varepsilon^2 u_2(\mathbf{x},\mathbf{y}) + \dots, \tag{4}$$

where the functions $u_i(\mathbf{x},\mathbf{y})$ are periodic in $\mathbf{y}$. The fact that

$$\mathbf{y} = \frac{\mathbf{x}}{\varepsilon},$$

implies that

$$\nabla = \nabla_x + \varepsilon^{-1}\nabla_y. \tag{5}$$

The substitution of expansion (4) into problem $(\mathcal{P}^\varepsilon)$ and use of the chain rule (5) leads to a sequence of problems in powers of ε to be solved.

(i) To $O(\varepsilon^{-2})$,

$$\nabla_y \cdot (\boldsymbol{k}^\varepsilon \nabla_y u_0) = 0. \tag{6}$$

Using the solvability condition in [10] (the average of the right hand side of (6) is zero),

$$u_0(\mathbf{x},\mathbf{y}) = u_0(\mathbf{x}). \tag{7}$$

(ii) To $O(\varepsilon^{-1})$ and from result (7), we can write

$$\nabla_y \cdot (\boldsymbol{k}^\varepsilon \nabla_y u_1) = -\nabla_y \cdot (\boldsymbol{k}^\varepsilon \nabla_x u_0)\,.$$

By the $\mathbf{y}$-periodicity of $\boldsymbol{k}^\varepsilon$ and the solvability condition, the last equation has a Y-periodic solution which is unique up to an additive constant. Since the problem is linear and $u_0 = u_0(\mathbf{x})$, then u_1 can be written as

$$u_1(\mathbf{x},\mathbf{y}) = \boldsymbol{\chi}(\mathbf{y}) \cdot \nabla_x u_0(\mathbf{x}), \tag{8}$$

where $\boldsymbol{\chi}(\mathbf{y})$ is a Y-periodic vector function with $\langle \boldsymbol{\chi} \rangle = 0$ ($\langle \bullet \rangle$ denotes the volume average over the periodic cell), satisfying the local problem

$$\begin{cases} \nabla_y \cdot (\boldsymbol{k}^\varepsilon \nabla_y (\boldsymbol{\chi} + \mathbf{y})) = 0 & \text{in } Y \setminus \Gamma, \\ [\![\boldsymbol{\chi}]\!] = 0 & \text{on } \Gamma, \\ [\![(\boldsymbol{k}^\varepsilon \nabla_y (\boldsymbol{\chi} + \mathbf{y})) \cdot \mathbf{n}]\!] = 0 & \text{on } \Gamma. \end{cases} \tag{9}$$

(iii) To $O(\varepsilon^0)$, using results (7), (8), and applying the volume average operator, it is obtained that $u_0(\mathbf{x})$ is the solution of the homogenized problem

$$(\mathcal{P}^h) \begin{cases} \langle \rho^\varepsilon c^\varepsilon \rangle \frac{\partial u_0}{\partial t} = \nabla_x \cdot \left(\hat{\boldsymbol{k}} \nabla_x u_0 \right) - \langle g^\varepsilon \rangle u_0 + \langle f^\varepsilon \rangle & \text{in } \Omega_\varepsilon \times (0,T), \\ \hat{\boldsymbol{k}} \nabla_x u_0 \cdot \mathbf{n} = \boldsymbol{k}^g \nabla_x u^g \cdot \mathbf{n} & \text{on } \partial\Omega_\varepsilon \times (0,T), \\ u_0 = u^g & \text{on } \partial\Omega_\varepsilon \times (0,T), \end{cases} \tag{10}$$

where

$$\hat{\boldsymbol{k}} = \langle \boldsymbol{k}^\varepsilon + \boldsymbol{k}^\varepsilon \nabla_y \boldsymbol{\chi} \rangle \tag{11}$$

denotes the effective thermal conductivity tensor and

$$\begin{aligned} \langle g^\varepsilon \rangle &= \rho_b c_b \omega_b^g \frac{|Y_g|}{|Y|} + \rho_b c_b \omega_b^t \frac{|Y_t|}{|Y|}, \\ \langle f^\varepsilon \rangle &= \left(q_m^g + \rho_b c_b \omega_b^g u_a \right) \frac{|Y_g|}{|Y|} + \left(q_m^t + \rho_b c_b \omega_b^t u_a \right) \frac{|Y_t|}{|Y|}, \end{aligned}$$

with $|\bullet|$ denoting the volume measure of $\bullet$.

4.1.1 Solution of the cell problem

In order to have problem $(\mathcal{P}^h)$ completely determined, we need to find the effective property $\hat{\boldsymbol{k}}$. From equation (11) it is noted that it is first necessary to find the solution $\boldsymbol{\chi}$ of the cell problem (9). Here, we adopt a procedure similar to that given in [12]. In this sense, the cell problem (9) is written (in index notation) as the following two problems

$$(\mathcal{L}_p) \quad \begin{cases} k_{ij}^{(\gamma)} \frac{\partial^2 \chi_p^{(\gamma)}}{\partial y_i \partial y_j} = 0 & \text{in} \quad Y_\gamma, \\ [\![\chi_p]\!] = 0 & \text{on} \quad \Gamma, \\ \left[\!\!\left[k_{ij} \frac{\partial \chi_p}{\partial y_j} n_i \right]\!\!\right] = - [\![k_{ip} n_i]\!] & \text{on} \quad \Gamma, \end{cases} \tag{12}$$

with $p = 1, 2$; $\gamma = g, c$ and $i, j = 1, 2$. Both problems in (12) can be conveniently rewritten as follows

$$(\mathcal{L}_p) \quad \begin{cases} \Delta \chi_p^{(\gamma)} = \alpha_p^\gamma \frac{\partial^2 \chi_p^{(\gamma)}}{\partial y_{\frac{2}{p}}^2} & \text{in } Y_\gamma, \\ [\![\chi_p]\!] = 0 & \text{on } \Gamma, \\ \left[\!\!\left[k_{pp} \frac{\partial \chi_p}{\partial y_i} n_i \right]\!\!\right] = - [\![k_{ip} n_i]\!] + \left[\!\!\left[k_{pp} \alpha_p \frac{\partial \chi_2}{\partial y_{\frac{2}{p}}} n_{\frac{2}{p}} \right]\!\!\right] & \text{on } \Gamma, \end{cases} \tag{13}$$

where

$$\alpha_p^\gamma = \begin{cases} 1 - k_2^\gamma/k_1^\gamma & \text{for } p = 1, \\ 1 - k_1^\gamma/k_2^\gamma & \text{for } p = 2. \end{cases}$$

In (13) no summation on the index p is performed. Moreover, $n_{\frac{2}{p}} = n_2$ and $y_{\frac{2}{p}} = y_2$ for $p = 1$, and $n_{\frac{2}{p}} = n_1$ and $y_{\frac{2}{p}} = y_1$ for $p = 2$. Here we note that the problem formulation (13) slightly differs of the one inferred in [12]. However, its solution is found similarly as in [12]. In this way, each α_p^γ is written in terms of one small parameter β and known integers $L_{\gamma k}^p$ $(k = 1, 2, 3)$ as follows

$$\alpha_p^\gamma = L_{\gamma 1}^p \beta + L_{\gamma 2}^p \beta^2 + L_{\gamma 3}^p \beta^3. \tag{14}$$

Moreover, the following ansatz is proposed

$$\chi_p^{(\gamma)} = {}_0\chi_p^{(\gamma)} + {}_1\chi_p^{(\gamma)} \beta + {}_2\chi_p^{(\gamma)} \beta^3 + \ldots \tag{15}$$

Then, substituting (14) and (15) into (13) and equaling in powers of β, problem (13) rewrites as the following pair of recurrent problems,

$$\left(\mathcal{L}_p^0\right) \quad \begin{cases} \Delta({}_0\chi_p^{(\gamma)}) = 0 & \text{in } Y_\gamma, \\ [\![{}_0\chi_p]\!] = 0 & \text{on } \Gamma, \\ \left[\!\left[k_{pp} \frac{\partial({}_0\chi_p)}{\partial y_i} n_i \right]\!\right] = - [\![k_{ip} n_i]\!] & \text{on } \Gamma \end{cases} \tag{16}$$

and

$$\left(\mathcal{L}_p^1\right) \quad \begin{cases} \Delta({}_1\chi_p^{(\gamma)}) = L_{\gamma 1}^p \frac{\partial^2({}_0\chi_p^{(\gamma)})}{\partial y_{\frac{2}{p}}^2} & \text{in } Y_\gamma, \\ [\![{}_1\chi_p]\!] = 0 & \text{on } \Gamma, \\ \left[\!\left[k_{pp} \frac{\partial({}_1\chi_p)}{\partial y_i} n_i \right]\!\right] = \left[\!\left[k_{pp} L_1^p \frac{\partial({}_0\chi_p)}{\partial y_{\frac{2}{p}}} n_{\frac{2}{p}} \right]\!\right] & \text{on } \Gamma. \end{cases} \tag{17}$$

We remark that no summation on the index p is performed in Eqs. (16) and (17). For each p, the solution of (16)-(17) can be found by solving the following infinite linear systems for $\hat{\mathbf{A}}_p = (\hat{a}_1^p, \hat{a}_2^p, \ldots)^T$, $\hat{\mathbf{B}}_p = (\hat{b}_1^p, \hat{b}_2^p, \ldots)^T$ (see Appendix A),

$$\left(\mathcal{L}_p^0\right) \quad \left(\mathbf{I} + (-1)^{p+1} \xi_p \mathbf{W}_p\right) \hat{\mathbf{A}}_p = \mathbf{V}_p, \tag{18}$$

$$\left(\mathcal{L}_p^1\right) \quad \left(\mathbf{I} + (-1)^{p+1} \xi_p \mathbf{W}_p\right) \hat{\mathbf{B}}_p = \mathbf{Y}_p + \left(\mathbf{U}_p + (-1)^{p+1} \frac{L_{g1}^p}{4} \mathbf{W'}_p\right) \hat{\mathbf{A}}_p. \tag{19}$$

In order to determine the effective thermal conductivity $\hat{\boldsymbol{k}}$, it is necessary to truncate the systems (18)-(19) at an appropriate order N. In fact, only a_1^p, a_3^p and b_1^p will be needed (see Appendix B), given that

$$\hat{k}_{pp} = k_p^g \left(1 - (-1)^{p+1} 2\pi a_1^p\right) - (-1)^{p+1} \left(k_p^g - k_p^c\right) \pi R \lambda_p \beta. \tag{20}$$

4.2 Solution of the macroscopic problem

Once the effective coefficient is found, problems $(\mathcal{P}^i)$ and $(\mathcal{P}^h)$ can be solved. For this we first introduce the characteristic functions $\Phi_i \in \Omega_i$ $(i = m, f, g, \varepsilon)$, namely

$$\Phi_i = \begin{cases} 1 & \text{if } \mathbf{x} \in \Omega_i \\ 0 & \text{if } \mathbf{x} \notin \Omega_i \end{cases}$$

and define

$$\begin{aligned} \boldsymbol{k} &= \boldsymbol{k}^m \Phi_m + \boldsymbol{k}^g \Phi_g + \boldsymbol{k}^f \Phi_f + \hat{\boldsymbol{k}} \Phi_\varepsilon, \\ G &= g^m \Phi_m + g^g \Phi_g + g^f \Phi_f + \langle g^\varepsilon \rangle \, \Phi_\varepsilon, \\ F &= f^m \Phi_m + f^g \Phi_g + f^f \Phi_f + \langle f^\varepsilon \rangle \, \Phi_\varepsilon, \\ C &= \rho^m c^m \Phi_m + \rho^g c^g \Phi_g + \rho^f c^f \Phi_f + \langle \rho^\varepsilon c^\varepsilon \rangle \, \Phi_\varepsilon, \\ U &= u^m \Phi_m + u^g \Phi_g + u^f \Phi_f + u^\varepsilon \Phi_\varepsilon, \end{aligned}$$

where $g^i = \rho_b c_b \omega_b^i$, $f^i = q_m^i + \rho_b c_b \omega_b^i u_a$ for $i = m, g, f$ and

$$\langle \rho^\varepsilon c^\varepsilon \rangle = \rho^g c^g \frac{|Y_g|}{|Y|} + \rho^c c^c \frac{|Y_c|}{|Y|}.$$

Then, $(\mathcal{P}^i)$ and $(\mathcal{P}^h)$, can be merged into one single problem as follows,

$$(\mathcal{P}) \begin{cases} C \frac{\partial U}{\partial t} = \nabla_x \cdot (\boldsymbol{k} \nabla_x U) - GU + F & \text{in } \Omega, \\ -\boldsymbol{k}^f \nabla_x U \cdot \mathbf{n} = h \, (U - u_e) & \text{on } \partial\Omega^n, \\ U = u_p & \text{on } \partial\Omega^d, \end{cases} \tag{21}$$

with initial condition $U = \tilde{u}$. In order to find the solution of of problem $(\mathcal{P})$ we use ***FreeFem++***. In particular, equation (21) is written in its weak form and the involved functions are approximated by piecewise linear continuous finite elements. The existence, uniqueness and regularity of the problem weak solution $(\mathcal{P})$ can be proved by standard methods using the Lax-Milgram theorem [17].

5 RESULTS AND DISCUSSION

In the present section the internal and surface temperature of a cancerous breast are studied. The thermophysical parameters were taken from [18, 19, 20] and presented in Tab. 1. In particular, the data presented in Tab. 1 for the tumor and the glandular tissues refer to the specific portion they occupy in Ω_ε and not the entire tumor region. Moreover, h is set equal

Table 1: Thermophysical parameters

	Muscle	Gland	Fat	Tumor
$\boldsymbol{k}$ $(W/m\,°\text{C})$	$\text{diag}[0.48, 0.48]$	$\text{diag}[0.48, 0.48]$	$\text{diag}[0.21, 0.21]$	$\text{diag}[0.48, 0.48]$
ω_b $(1/s)$	0.0009	0.0006	0.0002	0.012
c $(J/kg\,°\text{C})$	3800	3770	2770	3852
ρ (kg/m^3)	1100	1050	930	1050
q_m (Wm^{-3})	700	700	400	

to 13.5 W/m°C, $u_a = u_p = 37$ °C, $u_e = 26$ °C, $\tilde{u} = 37$ °C, $c_b = 4200\ J/kg$°C [8] and $\rho_b = 1060\ kg/m^3$ [8]. The metabolic heat value for different tumor sizes is calculated using the following relation: $q_m^t = C/(468.6\ln(100D) + 50)$ ([7]), where $C = 3.27 \times 10^6\ Wday/m^3$ and D is the tumor diameter. To mimic the *in situ* heterogeneous tumor, a circle with radius $r = 0.01\ m$ was embedded in the breast model at a depth of $d = 0.02\ m$ and a relative large tumor volume measure $|Y_t| = 0.7$ is considered in the cancerous region.

5.1 Isotropic case

As it can be observed in Tab. 1 the thermal conductivity tensor of the tumorous tissue presents an isotropic form. For this case, we can use the results in Section 4.1.1 making the corresponding changes. Figure 2 shows the temperature distribution of a cancerous breast when the thermal conductivity tensor $\boldsymbol{k}$ is isotropic for different depths and off-axis positions. As it

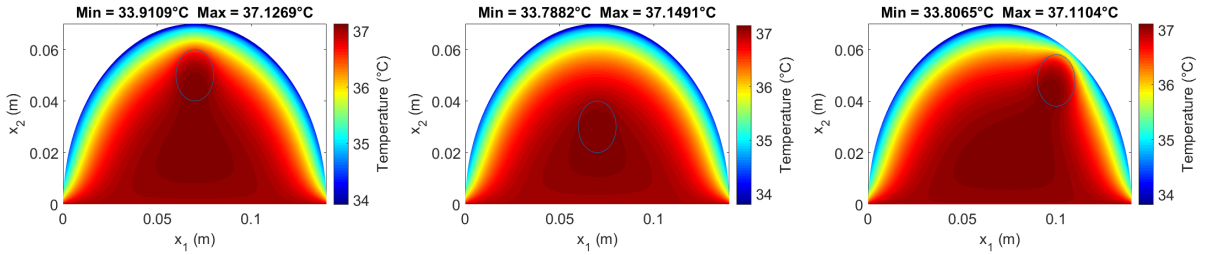

Figure 2: Temperature distribution of a cancerous breast tissue for different positions of the tumor.

can be noted temperature anomalies in the region where the tumor is located and on the breast surface near to the tumor location are observed. Moreover, depth and off-axis positions of the tumor affect the thermal distribution in the breast and the temperature profile on its boundary. Indeed, when the tumor is nearer to the boundary, the surface temperature increases. On the other hand, with the presence of Fig. 2, the authors would like to amend the figures reported in [21], which were wrongly printed. The reader could also refer to [9].

5.2 Anisotropic case

It is known that most soft biological tissues possess highly anisotropic properties. Furthermore, the importance of including anisotropic properties on tumors has been demonstrated in [13, 14]. In this sense, and given the lack of experimental data, we introduce the constant parameter δ such that the components of the conductivity tensor $\boldsymbol{k}^c$ are given by k_1^c and $k_2^c + \delta$. First, Fig. 3 shows the estimated the temperature difference ($\Delta u = u_{aniso} - u_{iso}$) in the breast domain between the temperature distributions of the isotropic (u_{iso}) and anisotropic (u_{aniso}) formulations for different values of δ. At a first glance it can be noted that near the tumor region surrounding it the thermal profile becomes distorted. In particular, the anisotropic model induces higher temperatures compared to the isotropic one. Moreover, the increment of the parameter δ is directly related to the augment of the breast temperature where major differences are perceived in the direction of the anisotropy. In fact, the increase in the temperature distribution is also visible on the breast surface near the tumor. As it can be observed in Fig. 4 the effect of the anisotropic assumption on the breast surface temperature distribution is illustrated. The core assumption of thermography is to find local breast surface temperature anomalies that points to a probable tumor site. Then, results in Fig. 4 show that the consideration of anisotropy in the thermal conductivity tensor constitutes one of the key factors to be considered in the

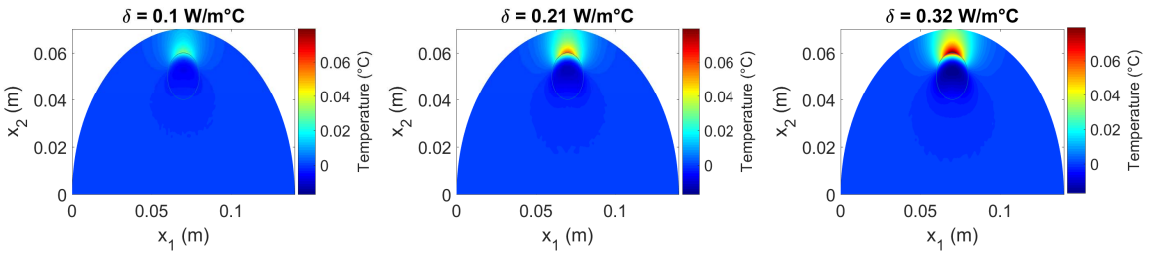

Figure 3: Estimated temperature difference between the isotropic and anisotropic models for different values of δ.

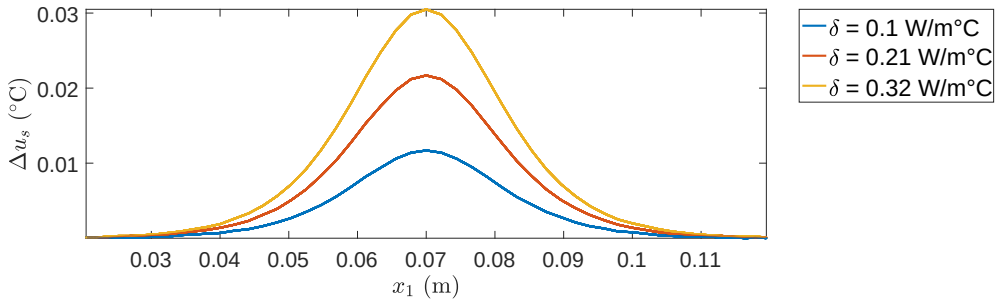

Figure 4: Estimated breast surface temperature for different values of δ.

study of cancerous breast thermal profiles, and therefore, for providing a helpful framework in the detection of breast tumors using thermography technique.

6 Conclusions

In the present work, the temperature distribution in a cross-section of a cancerous breast is studied by means of a semi-analyical approach combining asymptotic homogenization and finite element computations. The cross-section is supposed to be multilayered consisting of muscle, fat gland and a cancerous region embedded in the glandular tissue. It is also considered an anisotropic form for tumor's thermal conductivity. In particular, the cell problem for the periodically heterogeneous region is solved analytically by using an analogous procedure to that in [12], but formulating conveniently the cell problems. The assumption of anisotropy induces temperature profile alterations in the region near the tumor and on the breast surface and consequently, represent one of the key factors to be considered in the study of the surface temperature distribution of cancerous breasts.

The proposed approach facilitates a best understanding of the complex mechanism underlying the temperature profile on cancerous breasts by integrating mathematical and computational tools. Future research directions are the consideration of topological and hydraulic properties of the tumor microvasculature (see [22]) and the conception of a three-dimensional setting by using the results in [23].

The incorporation of the thermography technique in clinical proceedings may boost both sensitivity and specificity since no single tool provides excellent predictability.

ACKNOWLEDGMENTS

AR and LP are financially supported by INdAM. AR gratefully acknowledges the Program of Postdoctoral Scholarships of DGAPA from UNAM, Mexico. AG is financially supported by the Politecnico di Torino and the Fondazione CRT through the research program "La Ricerca dei

Talenti" (HR Excellence in Research). JM and RP acknowledges support from the Ministerio de Ciencia in Spain under the project reference DPI2014-58885-R. Thanks to the Project (7515) Métodos Físico-Matemáticos para el estudio de nuevos materiales y la propagación de ondas. Aplicaciones. Also, we thanks to Departamento de Matemáticas y Mecánica IIMAS-UNAM for their support and Ramiro Chávez Tovar and Ana Pérez Arteaga for computational assistance.

A SOLUTION OF THE CELL PROBLEM

The solution of the cell problem is sought by solving the following recurrent auxiliary cell problems (16) and (17). Problem (16) consists of finding a doubly-periodic harmonic function with null average over the periodic cell. Consequently, the method of complex variables in terms of two harmonic functions ${}_0\varphi_p^{(g)}(z)$ and ${}_0\psi_p^{(c)}(z)$ and the Kolosov-Muskhelishvili complex potentials are applicable (see [9] for further details). Once the harmonic functions ${}_0\chi_p^{(\gamma)}$ are known, the solution to problem (17) can be sought to satisfy a biharmonic equation with the same double periodicity, since the right-hand-side of Eq. (17) is harmonic. Following [12], the function ${}_1\chi_p^{(\gamma)}$ can be found by adapting Goursat's method, used in the context of plane elastic problems to solve the biharmonic equation in terms of two harmonic function ${}_1\varphi_p^{(g)}(z)$ and ${}_1\psi_p^{(c)}(z)$.

The complex potentials ${}_0\varphi_p^{(g)}$, ${}_0\psi_p^{(c)}$, ${}_1\varphi_p^{(g)}$ and ${}_1\psi_p^{(c)}$ are sought in the form

$$ {}_0\varphi_p^{(g)}(z) = a_0^p z + \sum_{k=1}^{\infty\ o} a_k^p \frac{\zeta^{(k-1)}(z)}{(k-1)!} \tag{22} $$

$$ {}_0\psi_p^{(c)}(z) = \sum_{k=1}^{\infty\ o} c_k^p z^k, \tag{23} $$

$$ {}_1\varphi_p^{(g)}(z) = \frac{L_{g1}^p}{4}\frac{\mathrm{d}({}_0\varphi_p^{(g)}(z))}{\mathrm{d}z}\bar{z} + b_0^p z + \sum_{k=1}^{\infty\ o}\left(b_k^p \frac{\zeta^{(k-1)}(z)}{(k-1)!} + a_k^p \frac{L_{g1}^p}{4}\frac{Q^{(k-1)}(z)}{(k-1)!}\right), \tag{24} $$

$$ {}_1\psi_p^{(c)}(z) = \frac{L_{c1}^p}{4}\frac{\mathrm{d}({}_0\psi_p^{(c)}(z))}{\mathrm{d}z}\bar{z} + \sum_{k=1}^{\infty\ o} d_k^p z^k, \tag{25} $$

where a_k^p, c_k^p, b_k^p and d_k^p are real coefficients to be determined, ζ represents the quasi-periodic Weierstrass functions of periods $w_1 = 1$ and $w_2 = i$ [**?**], Q represents the quasi-periodic Natanzon's function [**?**], $\zeta^{(k)}$ and $Q^{(k)}$ denote the k^{th} derivative of ζ and Q and the superscript o specifies that the sum is carried out over odd indices only. Using Legendre's relations, the quasi-periodicity of Q, the periodicity conditions for ${}_0\varphi_p$ and ${}_p\varphi_1$ are satisfied if

$$ a_0^p = (-1)^p a_1^p \pi \quad \text{and} \quad b_0^p = \frac{L_{g1}^p}{4}\left(\pi + (-1)^{p+1}\frac{5S_4}{\pi}\right) + (-1)^p b_1^p \pi, $$

respectively. Moreover, the Laurent series of $\zeta^{(k-1)}$ and $Q^{(k-1)}$ in zero are given by

$$ \frac{\zeta^{(k-1)}}{(k-1)!} = \frac{1}{z^k} - \sum_{l=1}^{\infty\ o} k\eta_{kl} z^l \quad \text{with } \eta_{kl} = \frac{(k+l-1)!}{k!l!} S_{k+l} \text{ for } k \geq 0 \text{ and } k \text{ odd}, $$

$$ \frac{Q^{(k-1)}(z)}{(k-1)!} = \sum_{l=1}^{\infty\ o} k\eta'_{kl} z^l \quad \text{with } \eta'_{kl} = \frac{(k+l)!}{k!l!} T_{k+l} \text{ for } k \geq 3 \text{ and } k \text{ odd}, $$

where S_k are the reticulate sums defined as $S_k = \sum_{w\in L^*} \frac{1}{w^k}$ ($k \geq 3$, k odd), $w = mw_1 + nw_2$ with $m, n \in \mathbb{Z}$ and L^* represents the lattice excluding $w = 0$, moreover $T_k = \sum_{w\in L^*} \frac{\bar{w}}{w^{k+1}}$.

Then, proposing the following ansatz for each problem $(\mathcal{L}_p^0)$ $(p = 1, 2)$,

$$(\mathcal{L}_1^0)\begin{cases} {}_0\chi_1^{(g)} = \mathcal{R}\left({}_0\varphi_1^{(g)}\right) \\ {}_0\chi_1^{(c)} = \mathcal{R}\left({}_0\psi_1^{(c)}\right) \end{cases} \quad \text{and} \quad (\mathcal{L}_2^0)\begin{cases} {}_0\chi_2^{(g)} = \mathcal{I}\left({}_0\varphi_2^{(g)}\right) \\ {}_0\chi_2^{(c)} = \mathcal{I}\left({}_0\psi_2^{(c)}\right) \end{cases} \tag{26}$$

where $\mathcal{R}$ and $\mathcal{I}$ define the real and imaginary parts of the involved functions. Moreover, for each problem $(\mathcal{L}_p^1)$ $(p = 1, 2)$,

$$(\mathcal{L}_1^1)\begin{cases} {}_1\chi_1^{(g)} = \mathcal{R}\left({}_1\varphi_1^{(g)}\right) \\ {}_1\chi_1^{(c)} = \mathcal{R}\left({}_1\psi_1^{(c)}\right) \end{cases} \quad \text{and} \quad (\mathcal{L}_2^1)\begin{cases} {}_1\chi_2^{(g)} = \mathcal{I}\left({}_1\varphi_2^{(g)}\right) \\ {}_1\chi_2^{(c)} = \mathcal{I}\left({}_1\psi_2^{(c)}\right) \end{cases} . \tag{27}$$

We substitute formulae (26), (27) into the interface conditions of (16), (17) respectively. Then, for each p, the solution of (16)-(17) can be found by solving the following recurrent infinite linear systems for $\hat{\mathbf{A}}_p = (\hat{a}_1^p, \hat{a}_2^p, \ldots)^T$ and $\hat{\mathbf{B}}_p = (\hat{b}_1^p, \hat{b}_2^p, \ldots)^T$,

$$\begin{aligned} &\left(\mathcal{L}_p^0\right) \quad \left(\mathbf{I} + (-1)^{p+1}\xi_p \mathbf{W}_p\right)\hat{\mathbf{A}}_p = \mathbf{V}_p, \\ &\left(\mathcal{L}_p^1\right) \quad \left(\mathbf{I} + (-1)^{p+1}\xi_p \mathbf{W}_p\right)\hat{\mathbf{B}}_p = \mathbf{Y}_p + \left(\mathbf{U}_p + (-1)^{p+1}\frac{L_{g1}^p}{4}\mathbf{W'}_p\right)\hat{\mathbf{A}}_p, \end{aligned}$$

with $\mathbf{V}_p = ((-1)^{p+1}R, 0, \ldots)^T$, $\mathbf{Y}_p = (N_{p1}R, 0, \ldots)^T$, $\mathbf{U}_p = \text{diagsup}\left\{N_{pl}^2\sqrt{l(l+2)}\right\} + \text{diag}\left\{N_{pl}^0 l\right\} + \text{diaginf}\left\{N_{pl}^{-2}\sqrt{l(l-2)}\right\}$, $\xi_p = \frac{k_p^g - k_p^c}{k_p^g + k_p^c}$ and

$$\mathbf{W}_p = \begin{cases} (-1)^{p+1}\pi R^2 & \text{for } k+l = 2, \\ \sum_{k=1}^{\infty}{}^{o} \sqrt{kl}\eta_{kl}R^{k+l} & \text{for } k+l > 2, \end{cases} \quad \mathbf{W'}_p = \begin{cases} \left(\pi + (-1)^{p+1}\frac{5S_4}{\pi}\right)R^2 & \text{for } k+l = 2, \\ \sum_{k=1}^{\infty}{}^{o} \sqrt{kl}\eta'_{kl}R^{k+l} & \text{for } k+l > 2. \end{cases}$$

Note that, given a tridiagonal matrix, diagsup denotes the "line" of entries of the matrix that stays above the principal diagonal. Analogously, diaginf indicates the "line" of entries that finds itself below the principal diagonal. Furthermore, defining $\xi_p^g = \frac{k_p^g L_{g1}^p}{k_p^g + k_p^c}$ and $\xi_p^c = \left(1 + \frac{\delta_{1l}}{2}\right)\frac{k_p^c L_{21}^p}{k_p^g + k_p^c}$,

$$\begin{aligned} N_{pl} &= \frac{L_{g1}^p}{4} + \xi_p^g - \xi_p^c \\ N_{pl}^{-2} &= \frac{1}{2}\left(\frac{L_{g1}^p}{2} + \frac{\xi_p^g}{l}\right) \\ N_{pl}^0 &= -\frac{\xi_p^{-1}L_{g1}^p}{4l}\delta_{1l} + \frac{\xi_p^g}{2l}\left[1 - \xi_p^{-1}(1+\delta_{1l})\right] + \frac{\xi_p^c}{l}(1+\xi_p^{-1}) \\ N_{pl}^2 &= \frac{1}{2}\left(\frac{L_{g1}^p}{2} - \frac{\bar{\xi}_p^g}{l}\right) \quad \text{with } \bar{\xi}_p^g = \frac{k_p^g L_{g1}^p}{k_p^g - k_p^c}. \end{aligned}$$

B ANISOTROPIC EFFECTIVE COEFFICIENTS

Using Green's theorem

$$\hat{k}_{pp} = k_p^g\,|Y_g| + k_p^c\,|Y_c| - \left(k_p^g - k_p^c\right)\int_\Gamma {}_0\chi_p^g \mathrm{d}y_{\frac{2}{p}} \tag{28}$$

and from (26), the effective coefficients for the isotropic case are given by

$$\hat{k}_{pp} = k_p^g \left(1 - (-1)^{p+1} 2\pi a_1^p\right).$$

Now, in the anisotropic case we can truncate to order β in (28),

$$\hat{k}_{pp} = k_p^g \left|Y_g\right| + k_p^c \left|Y_c\right| - \left(k_p^g - k_p^c\right) \int_\Gamma \left({}_0\chi_p^g + {}_1\chi_p^g \beta\right) \mathrm{d}y_{\frac{2}{p}}. \tag{29}$$

Then, from (27)

$$\hat{k}_{pp} = k_p^g \left(1 - (-1)^{p+1} 2\pi a_1^p\right) - (-1)^{p+1} \left(k_p^g - k_p^c\right) \lambda_p \pi R \beta,$$

where

$$\lambda_p = -\left(\frac{L_{g1}^p}{4} + \xi_p^{-1} N_{p1}\right) R + \left((-1)^{p+1} \frac{L_{g1}^p \xi_p^{-1}}{4} - \xi_p^{-1} N_{p1}^0\right) a_1^p R^{-1} + \left(1 + \xi_p^{-1}\right) b_1^p R^{-1} + \left(\frac{3 L_{g1}^p \xi_p^{-1}}{4} - 3\xi_p^{-1} N_{p1}^2\right) a_3^p R^{-3}.$$

REFERENCES

[1] Y. Jayasinghe, P. S. Simmons, Fibroadenomas in adolescence. *Current Opinion in Obstetrics Gynecology*. **21**, 402–406, 2009.

[2] M. Salhab, L. G. Keith, M. Laguens, W. Reeves, K. Mokbel. The potential role of dynamic thermal analysis in breast cancer detection. *International Seminars in Surgical Oncology*, **5**, 1-5, 2006.

[3] L. F. Silva, A. A. Santos, R. S. Bravo, A. C. Silva, D. C. Muchaluat-Saade, A. Conci, Hybrid analysis for indicating patients with breast cancer using temperature time series. *Computer Methods and Programs in Biomedicine*, **130**, 142–153, 2016.

[4] M. Gautherie, Thermopathology of breast cancer: measurement and analysis. *Annals of the New York Academy of Sciences*, **335**, 383–415, 1980.

[5] D. Kennedy, T. Lee, D. Seely, A comparative review of thermography as a breast cancer screening technique. *Integrative Cancer Therapies*, **8**(1), 9–16, 2009.

[6] H. Pennes, Analysis of tissue and arterial blood temperatures in the resting human forearm. *Journal of Applied Physiology*, **1**, 93–122, 1948.

[7] L. Jiang, W. Zhan, M. H. Loew, Modeling static and dynamic thermography of the human breast under elastic deformation. *Physics in Medicine & Biology*, **56**(1), 187–202, 2011.

[8] L. A. Bezerra, M. M. Oliveira, T. L. Rolim, A. Conci, F. G. S. Santos, P. R. M. Lyra, R. C. F. Lima, Estimation of breast tumor thermal properties using infrared images. *Signal Process*, **93**(10), 2851–2863, 2013.

[9] A. Ramírez-Torres, R. Rodríguez-Ramos, F. J. Sabina, C. García-Reimbert, R. Penta, J. Merodio, R. Guinovart-Díaz, J. Bravo-Castillero, A. Conci, L. Preziosi, The role of malignant tissue on the thermal distribution of cancerous breast. *Journal of Theoretical Biology*, **426**, 152–161, 2017.

[10] N. Bakhalov, G. Panasenko, *Homogenisation: Averaging processes in periodic media*. Kluwer Academic Publishers, Dordrecht, 1989.

[11] E. Sanchez-Palencia, *Non-Homogeneous Media And Vibration Theory*. Springer-Verlag, Berlin, 1980.

[12] E. López-López, F. J. Sabina, R. Guinovart-Díaz, J. Bravo-Castillero, R. Rodríguez-Ramos, Overall longitudinal shear elastic modulus of a 1-3 composite with anisotropic constituents. *International Journal of Solids and Structures*, **50**, 2573–2583, 2013.

[13] M. C. Colombo, C. Giverso, E. Faggiano, C. Boffano, F. Acerbi, P. Ciarletta, Towards the personalized treatment of glioblastoma: Integrating patient-specific clinical data in a continuous mechanical model. *PLoS ONE*, **10**(7), e0132887, 2015.

[14] A. Swan, T. Hillen, J. C. Bowman, A. D. Murtha, A patient-specific anisotropic diffusion model for brain tumour spread. *Bulletin of Mathematical Biology*, 1–33, 2017.

[15] A. A. Wahab, M. I. M. Salim, M. A. Ahamat, N. A. Manaf, J. Yunus, K. W. Lai, Thermal distribution analysis of three-dimensional tumor-embedded breast models with different breast density compositions. *Medical & Biological Engineering & Computing*, **54**, 1363–1373, 2015.

[16] R. M. Youngson, *Collins dictionary of Medicine fourth edition*, 2005.

[17] S. Salsa, *Patial Differential Equations in Action - From Modelling to Theory*. Springer-Verlag Ialia, Milan, 2008.

[18] E. Y. Ng, N. M. Sudharsan, An improved three-dimensional direct numerical modelling and thermal analysis of a female breast with tumour. *Proceedings of the Institution of Mechanical Engineers, Part H: Journal of Engineering in Medicine*, **215**(1), 25–37, 2001.

[19] A. Amri, A. Saidane, S. Pulko, Thermal analysis of a three-dimensional breast model with embedded tumour using the transmission line matrix (TLM) method. *Computers in Biology and Medicine*, **41**(2), 76–86, 2011.

[20] M. P. Cetingul, C. Herman, A heat transfer model of skin tissue for the detection of lesions: Sensitivity analysis. *Physics in Medicine and Biology*, **55**(19), 5933–5951, 2010.

[21] A. Ramírez-Torres, R. Rodríguez-Ramos, A. Conci, F. J. Sabina, C. García-Reimbert, L. Preziosi, J. Merodio, F. Lebon. A Semi-Analytical Heterogeneous Model for Thermal Analysis of Cancerous Breasts. Ng, E. Y. & Etehadtavakol, M. eds. *Application of Infrared to Biomedical Sciences*, 175–190. Springer Singapore, 2017.

[22] R. Penta, D. Ambrosi, The role of the microvascular tortuosity in tumor transport phenomena. *Journal of Theoretical Biology*, **364**, 80–97, 2015.

[23] R. Penta, A. Gerisch, Investigation of the potential of asymptotic homogenization for elastic composites via a three-dimensional computational study. *Computing and Visualization in Science*, **17**(4), 185–201, 2015.

[24] M. Abramowitz, I. A. Stegun, eds. *Handbook of Mathematical Functions with Formulas, Graphs, and Mathematical Tables. Applied Mathematics Series*. Washington D.C.; New York: United States Department of Commerce, National Bureau of Standards; Dover Publications, 1983.